Journal of Vegetation Science

IAVS

METHODOLOGICAL ARTICLE OPEN ACCESS

Pixels and Patterns in the Sand: Decoding Coastal Dune Habitats With Multi-Resolution CNNs

Emilia Pafumi[1,2,3] | Claudia Angiolini[2,3] | Giovanni Bacaro[1] | Leopoldo de Simone[2] | Emanuele Fanfarillo[2,3] | Tiberio Fiaschi[2] | Duccio Rocchini[4] | Elisa Thouverai[1] | Simona Maccherini[2,3]

[1]Department of Life Sciences, University of Trieste, Trieste, Italy | [2]Department of Life Sciences, University of Siena, Siena, Italy | [3]NBFC, National Biodiversity Future Center, Palermo, Italy | [4]BIOME Lab, Department of Biological, Geological and Environmental Sciences, Alma Mater Studiorum University of Bologna, Bologna, Italy

Correspondence: Emilia Pafumi (emilia.pafumi@units.it)

Received: 14 November 2025 | **Revised:** 4 June 2026 | **Accepted:** 5 August 2026

Coordinating Editor: Sebastian Schmidtlein

Keywords: biodiversity | coastal dunes | convolutional neural networks | deep learning | habitat mapping | remote sensing | spatial resolution

ABSTRACT

Aims: Mapping coastal dune habitats through remote sensing is crucial for biodiversity conservation, but it is challenging due to the small and fragmented nature of habitat patches relative to the spatial resolution of available imagery. Convolutional neural networks (CNNs), by leveraging both spectral and spatial information, offer a promising solution, but their application to coastal dunes remains limited. This study evaluates CNN performance for coastal dune habitat mapping using remote sensing data with varying spatial resolutions, testing how spatial resolution influences mapping accuracy and assessing the effect of including additional spectral bands beyond RGB.

Location: Coastal sand dunes in Maremma Regional Park, Tuscany, Italy.

Methods: Ground truth data were collected in 4-m^2 plots and supplemented with photo-interpreted patches, representing five classes: shifting dunes (EUNIS habitat N14), dune grasslands (N16), dune scrubs (N1B), bare sand, and sea. Four remote sensing datasets with varying spatial resolution were used: unmanned aerial vehicle (UAV; 0.02 m), airborne (0.20 m), Google Earth (0.30 m), and WorldView-3 imagery (0.40 m). For each remote sensing dataset, one CNN was trained on RGB imagery and, where additional spectral bands were available, a second CNN was trained on multispectral imagery.

Results: Most maps achieved high accuracy, confirming the effectiveness of CNNs for habitat mapping. Accuracy of RGB-derived maps declined with coarser resolution, from UAV (88%) to airborne (86%), Google Earth (80%), and WorldView-3 (38%). Including additional spectral bands had varying effects on accuracy (+6 percentage points for UAV, +7 for airborne, +35 for WorldView-3). Among habitats, dune scrubs were mapped most accurately, whereas shifting dunes were often confused with bare sand.

Conclusions: These findings underscore the value of very high-resolution imagery for habitat mapping with CNNs, suggesting that even Google Earth imagery can support broader scale applications when UAV or airborne data are unavailable.

1 | Introduction

Biodiversity mapping is a crucial task: although maps cannot faithfully represent reality, they serve essential practical purposes, such as guiding conservation efforts (Malavasi 2020). Habitat maps are particularly important in Europe, where many conservation policies, including the Habitats Directive (92/43/EEC; EEC 1992), require the identification and mapping of habitats as key units for protection. Remote sensing, by providing quantitative data over large spatial and temporal scales, has significantly advanced habitat mapping (Kerry et al. 2022). However, the suitability of remote sensing data remains strongly dependent on spectral, spatial, and temporal resolution: fine habitat differentiation generally requires multiple spectral bands to improve spectral separability, but this often comes at the expense of spatial detail or temporal frequency, which are relevant for complex landscapes (Corbane et al. 2015).

Coastal dune habitats are both highly threatened and challenging to map, due to their typically small and fragmented patches (Acosta et al. 2007). Recent studies have explored automatic approaches for dune habitat mapping, testing remote sensing data with varying spatial resolutions (Delbosc et al. 2021). The highest detail is currently provided by unmanned aerial vehicles (UAVs), which have been used to map land cover (Suo et al. 2019), plant communities (Agrillo et al. 2023; Cruz et al. 2023; De Giglio et al. 2019; Innangi et al. 2025), and even single species (Belcore et al. 2024; Innangi et al. 2023; Marzialetti et al. 2021). However, these studies are limited to a local scale, and it remains critical to assess the trade-off between spatial resolution and broader-scale applicability. Free satellite data only allow for mapping broad land cover classes (Latella et al. 2021; Marzialetti et al. 2019), whereas commercial satellites often enable more accurate mapping but are constrained by high acquisition costs (De Giglio et al. 2017; Pafumi et al. 2025). Recently, free Google Earth imagery has also been tested for specific vegetation types, such as bamboo forests (Watanabe et al. 2020) or scrub habitats (Guirado et al. 2017). However, its limited spectral information (RGB only) necessitates advanced classification methods for distinguishing habitats.

In recent years, machine learning has opened up new possibilities for ecological applications (Cipriano et al. 2025), especially in remote sensing (Cresson 2020). Among these methods, deep learning stands out for its ability to automatically extract complex features from raw data (LeCun et al. 2015). Specifically, convolutional neural networks (CNNs) are well suited for image classification tasks, as they exploit the hierarchical structure of images to extract high-level features (e.g., edges and patterns) from low-level inputs (e.g., pixel intensities), thus leveraging both spectral information and spatial context and improving ecological mapping performance (Kattenborn et al. 2019). The effectiveness of CNNs has been demonstrated in various applications to vegetation remote sensing (Kattenborn et al. 2021), especially with very high-resolution data, like UAV (Schiefer et al. 2020) or airborne imagery (Carbonneau et al. 2020). However, few studies have systematically assessed how CNN performance varies with spatial resolution, with most studies simulating coarser-resolution imagery from UAV data (e.g., Fromm et al. 2019; Schiefer et al. 2020; Saltiel et al. 2022), rather than comparing multiple real data sources. Moreover, the role of spectral resolution remains unclear (Kattenborn et al. 2021), as high-quality results can often be achieved using RGB data alone (e.g., Zhao et al. 2019; Nezami et al. 2020). Despite their growing use, CNNs remain poorly explored in the context of coastal dune habitats (Pérez-Carabaza et al. 2021; Lansu et al. 2025).

This study addresses this gap by focusing primarily on the issue of spatial resolution, which directly affects the ability of CNNs to extract fine-scale features (Schiefer et al. 2020), and secondarily on the role of spectral information. In particular, we test CNN-based habitat mapping in coastal dunes across four remote sensing datasets with decreasing spatial resolution: UAV imagery (0.02 m), airborne imagery (0.20 m), Google Earth imagery (0.30 m), and WorldView-3 satellite imagery (0.40 m). For each dataset, we assess CNN performance using RGB bands only and then test the added value of including additional spectral bands, where available.

2 | Materials and Methods

2.1 | Study Area

The study was carried out at the sandy beach of Collelungo in Tuscany (Italy; Figure 1). The Collelungo beach extends for ca. 7 km between the Ombrone river mouth in the northwest and the rocky shores southeast of the Uccellina Mountains. In the northwestern portion, the shoreline has been affected by coastal erosion, whereas in the southern section (starting ca. 5 km from the river mouth), it is in a condition of dynamic equilibrium, which determines the large width (about 150 m) and the slight slope (< 2%) (Nourisson and Scapini 2015; Pranzini et al. 2024). The area considered in this study (centroid coordinates: 42.634845° N, 11.072753° E) covers ca. 4 ha and is located in the stable portion of Collelungo beach.

The site is inside the Maremma Regional Park and the Special Area of Conservation "Dune costiere del Parco dell'Uccellina" (IT51A0015). The climate is Mediterranean, with an upper meso-mediterranean thermotype and an upper dry ombrotype (Pesaresi et al. 2017). Vegetation follows the typical coastal dune zonation, with annual vegetation of drift lines closer to the sea, mainly composed of nitrophilous pioneer species such as *Cakile maritima* and *Salsola tragus*, followed by shifting dunes, which are strongly associated with the dune-building perennial species *Calamagrostis arenaria* subsp. *arundinacea*. The fixed dune sector is characterized by stable dune grasslands, which show the highest species richness, including therophytes such as *Daucus pumilus*, *Festuca fasciculata*, *Ononis variegata*, and *Silene canescens*. Dune scrubs dominated by *Juniperus macrocarpa* occur intermixed with the grassland and in the inland part of the zonation, before the development of a large *Pinus* spp. plantation (Acosta et al. 2007; Beccari et al. 2024; Sarmati et al. 2025; Tordoni et al. 2019, 2021).

Due to the protection measures implemented by the Regional Park, anthropogenic pressure is generally limited in the area. Although seasonal recreational use occurs in Collelungo beach, the site considered in this study is less affected due to its distance from the main points of access to the beach.

Previous studies carried out in this area mainly described patterns of dune vegetation and the factors influencing it (e.g., Sarmati et al. 2025), analyzed arthropod biodiversity (Nourisson and Scapini 2015), and tested satellite data for vegetation

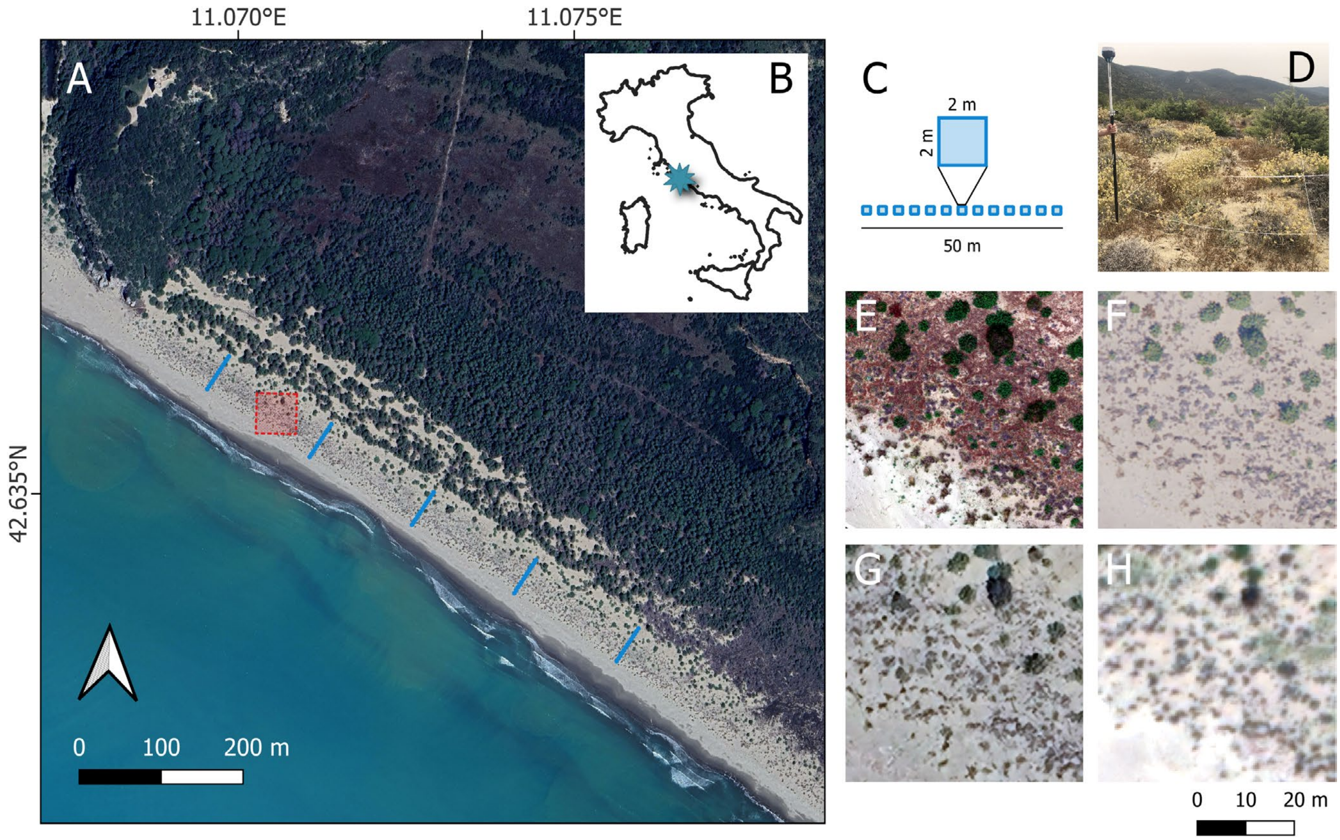

FIGURE 1 | Study area with field surveyed transects represented in blue (A), its position in Italy (B), a transect scheme (C), an example of surveyed plot (D) and close-up views of the remote sensing datasets used: UAV (E), airborne (F), Google Earth (G), and WorldView-3 (H). The area in the close-up views is indicated with a red square in A.

mapping (Pafumi et al. 2025), finding in general a good conservation status of the coastal dune system.

2.2 | Ground Truth Data

Ground truth data were collected during vegetation surveys in June 2024 over an area of ca. 4 ha. Five transects of fixed length (50 m) were placed perpendicularly to the coastline at 150 m from one another, with the first transect located 100 m from the beginning of the beach (Appendix S13). Along each transect, 13 square plots of 2 m × 2 m were placed, each at 4 m from the other, for a total of 65 plots. We measured coordinates at the top-left and bottom-right vertices of each plot along the sea-upland direction of each transect. Two EMLID Reach RS2 GNSS units were used for this purpose, one as a base station and one as a rover, connected for real-time kinematic (RTK) survey with a local accuracy of 0.001 m. As network communication in the area was insufficient, acquired coordinates were subsequently used for a post-processed kinematic (PPK) survey using the EMLID Studio software. The coordinates were calculated in the WGS84 reference system (EPSG: 4326), with PPK processing based on RTCM3 positional data of the Leica SmartNet network of reference stations (GROK site, with a baseline of approximately 18 km). After PPK corrections, plot coordinates had an RMS horizontal accuracy of less than 1 cm.

In each plot, vascular plant species occurrence and abundance (visually estimated % cover) were recorded. Plots were assigned to EUNIS habitats at level 3 of the classification hierarchy based on their species composition using the EUNIS Expert System (Bruelheide et al. 2021; Chytrý et al. 2020). Three habitats were considered: "Mediterranean, Macaronesian and Black Sea shifting coastal dune" (N14), "Mediterranean and Macaronesian coastal dune grassland (grey dune)" (N16), and "Mediterranean and Black Sea coastal dune scrub" (N1B). Habitat N14 develops on the first part of the coastal dune zonation and is characterized by a sparse vegetation cover, dominated by *Calamagrostis arenaria* subsp. *arundinacea*. Habitat N16, occurring on stable dunes, shows a denser cover and a high diversity of graminoids and herbs, usually dominated by *Crucianella maritima* and characterized by other diagnostic species including *Cutandia maritima*, *Ononis variegata* and *Silene canescens*. Finally, habitat N1B is represented by scrubs on stable dunes, dominated by *Juniperus oxycedrus* and other shrub species such as *Phillyrea angustifolia* and *Pistacia lentiscus* (Chytrý et al. 2020). A more detailed description of the EUNIS habitats considered in this study is reported in Appendix S11. Plots not assigned to any habitat or classified into other habitat types (specifically, N12—"Mediterranean and Black Sea sand beach," N1G—"Mediterranean coniferous coastal dune forest," and "Sb—Dwarf-shrub vegetation") were excluded from the reference dataset, as their number was too small to be considered in the analysis.

To improve the ground truth dataset and compensate for class imbalance, additional 2 m × 2 m squares were identified through photo interpretation of the highest-resolution image. The final dataset consisted of 500 square patches assigned to five classes: habitat N14, N16, N1B, bare sand, and sea (100 patches per class, except for the sea class, which was not covered by the UAV flight and only partially covered by the WorldView-3 image). The total number of pixels belonging to each class is reported in Appendix S12.

A workflow scheme of the analyses, from data collection to CNN segmentation, is provided in Figure 2.

2.3 | Remote Sensing Data Collection and Preprocessing

2.3.1 | UAV Imagery

The UAV photogrammetric survey was carried out on June 20, 2024, simultaneously with the vegetation surveys. This study adopted a low-altitude UAV, the DJI Matrice 300 RTK, equipped with the MicaSense Altum-PT multispectral camera (MicaSense Inc., Seattle, WA, USA). We used five out of seven sensors of the camera, each with a resolution of 2064 × 1544 pixels (≈3.2 MP per band), covering five discrete spectral bands: blue (center 475 nm, bandwidth 32 nm), green (560 nm, 27 nm), red (668 nm, 14 nm), red edge (717 nm, 12 nm), and near-infrared (842 nm, 57 nm). Prior to the flight, we placed the calibrated reflectance panel CRP2 on a flat, leveled surface within the mapping area. We used the Altum-PT to capture images of the panel under the same sunlight conditions as the planned survey, allowing radiometric calibration of multispectral data. Simultaneously, the downwelling light sensor DLS2 was used to record irradiance and sun-angle data for subsequent correction in processing. Image acquisition was carried out between 1:00 and 2:00 PM (UTC + 2). The flying height was set at 45 m, achieving a ground sampling distance (GSD), or spatial resolution, of 1.94 cm/pixel. Both image frontal and side overlap were set at 75%, which is essential for the image matching algorithms in Structure-from-Motion software (Eltner et al. 2016). Before the acquisition of the images, six ground targets were distributed across the study area and surveyed; three were used as ground control points (GCP) and three as independent check points (CP). The coordinates of the center of each ground target were acquired using the same methodology as for the vegetation plots (see Section 2.2. Ground truth data).

After the flight, UAV data were processed in Agisoft Metashape Professional v 2.1.0, applying radiometric corrections to all the 1046 acquired images using both the reflectance panel and the DLS2 sensor data. After image alignment, a five-band orthomosaic was generated, with a final output size of 40,300 × 29,430 pixels. The orthomosaic was referenced in WGS84/UTM Zone 32N (EPSG: 32632), with a CP horizontal Root Mean Square Error (RMSE) of 2.46 cm.

2.3.2 | Airborne Imagery

An airborne orthophoto from August 25, 2023, was downloaded from the regional open dataset (Regione Toscana 2023). The image was acquired using Leica DMC4 and DMC3 sensors with four spectral bands, that is, red (580–660 nm), green (480–590 nm), blue (420–510 nm), and near-infrared (720–850 nm), with a spatial resolution of 0.20 m.

2.3.3 | Google Earth Imagery

RGB imagery was downloaded from Google Earth Pro 7.3.6 (Google 2025). Among the available images, the one with the closest date to the field surveys was chosen, that is, a Pléiades Neo satellite image from April 26, 2023, with a spatial resolution of 0.30 m (Airbus 2023). The image was exported from Google Earth Pro at an eye altitude of 1 km, corresponding to a pixel size of ca. 0.14 m. This finer export sampling does not imply an increase in the native spatial resolution of the source imagery.

2.3.4 | WorldView-3 Imagery

A multispectral image from the WorldView-3 satellite was acquired on May 16, 2019. The image includes one panchromatic band at 0.40 m spatial resolution (center wavelength: 649 nm) bundled with eight spectral bands at 1.60 m resolution: coastal blue (427 nm), blue (482 nm), green (547 nm), yellow (604 nm), red (660 nm), red-edge (723 nm), near-infrared 1 (824 nm), and near-infrared 2 (914 nm). Images were delivered at the 3D-level of processing, that is, orthorectified, sensor-corrected, and radiometrically corrected through dark offset subtraction and non-uniformity correction (Kuester 2016), with a reported geolocation accuracy < 3.0 m CE90.

To improve spatial resolution of WorldView-3 images, multispectral bands were pansharpened using the weighted Brovey algorithm implemented in GDAL (GDAL/OGR contributors 2026), with cubic resampling. To correct for a slight misalignment among datasets, the images were co-registered using the UAV imagery as reference. These steps were carried out in QGIS 3.40.8 (QGIS Development Team 2024).

2.4 | Semantic Segmentation Using CNNs

For the semantic segmentation of images into dune habitats, we applied CNNs based on a fully convolutional encoder-decoder architecture, adapted from the U-Net, a widely used model, specifically developed to perform well with few training images (Cresson 2020). U-Net is an encoder–decoder architecture which consists of a contracting path with convolutional layers, followed by a symmetric expanding path with transposed convolutions (Ronneberger et al. 2015). In this study, CNN architecture was optimized by testing different values of key parameters (i.e., number of layers, kernel sizes, stride). The final structure comprises three convolutional layers and three symmetric deconvolutional layers (Appendix S1). Convolutions use a 3 × 3 kernel with stride 1, padding "same," and HeNormal initialization to reduce the vanishing gradient and stabilize the network. To efficiently reduce and restore spatial dimensions in the UAV dataset, max pooling and transposed convolutions with a stride of 2 were employed, following the original U-Net architecture. For the other datasets, we used a stride 1 throughout the network

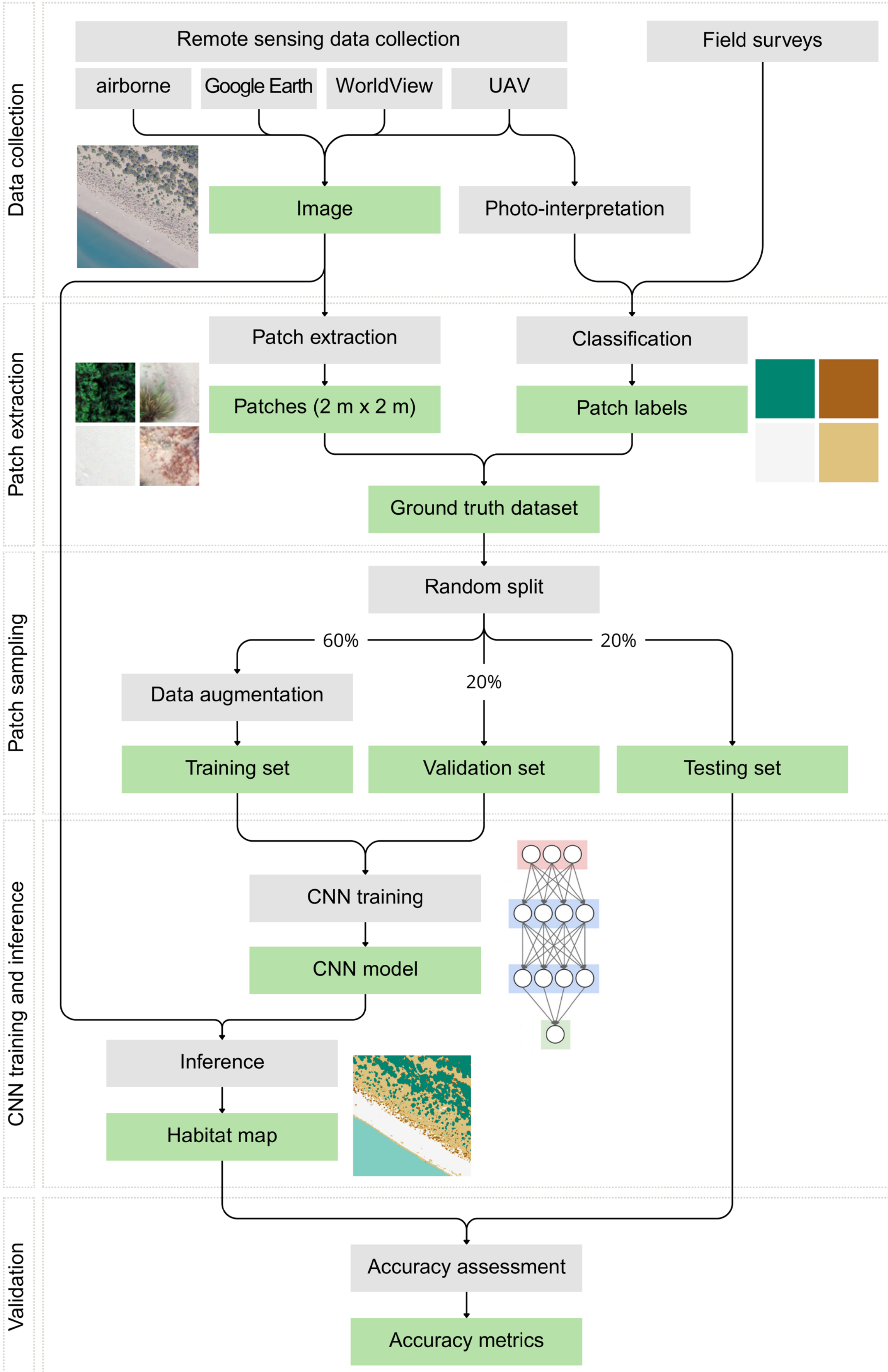

FIGURE 2 | Workflow scheme of the analyses.

and omitted pooling layers to avoid excessive downsampling. After each (de)convolutional layer, a ReLU activation and a batch normalization layer are applied, respectively, to compute the node output and reduce the internal covariate shift. A final argmax layer assigns each pixel to the most probable class.

To assess the effect of spatial resolution on classification accuracy, an independent CNN was trained for each remote sensing dataset using RGB images as input. Then, to assess the effect of adding spectral bands, additional CNNs were trained on multispectral images for all datasets except Google Earth, which only includes RGB bands, for a total of seven CNN models (Table 1, Appendix S2).

Patches were extracted with the same size as the field sampled plots (2 m × 2 m), thus with a different number of pixels according to the resolution of the data used. In each case, patches were randomly split into 60% training, 20% validation, and 20% testing. To artificially increase the training dataset, data augmentation was performed by adding two preprocessing layers (random flips and random rotations).

Models were trained for 50 epochs, using the Adam optimizer to minimize categorical cross-entropy loss, with a batch size of 8 and a learning rate of 0.0002. The training dataset consisted of 60 square patches for each class present in the reference ground truth dataset (Section 2.2).

TABLE 1 | List of CNNs trained in this study with different types of remote sensing data.

Data	Spatial resolution (m)	Input spectral bands	CNN
UAV	0.02	RGB	CNN-01
		Multispectral	CNN-02
Airborne	0.20	RGB	CNN-03
		Multispectral	CNN-04
Google Earth	0.30	RGB	CNN-05
WorldView-3	0.40	RGB	CNN-06
		Multispectral	CNN-07

CNNs were built and trained using Orfeo ToolBox TensorFlow (OTBTF; Cresson 2019), a remote module of the Orfeo ToolBox open source library (Grizonnet et al. 2017), that allows integration of deep learning models into remote sensing workflows using the TensorFlow platform for machine learning (Abadi et al. 2015) through its high-level Keras API (Chollet 2015). The *pyotb* library was used as a Python wrapper for Orfeo ToolBox applications, enabling seamless integration of OTB's remote sensing processing capabilities within Python-based workflows.

2.5 | Performance Assessment

The accuracy of the output maps was assessed using the test ground truth dataset, computing the following performance metrics: (1) overall accuracy, i.e., the percentage of correctly classified ground truth patches; (2) precision, i.e., the proportion of true positives over all classified positives, also known as user's accuracy in traditional remote sensing studies; (3) recall, i.e., the proportion of true positives over all actual positives, also known as producer's accuracy; (4) F1-score, i.e., the harmonic mean of precision and recall; (5) intersection over union (IoU), i.e., the ratio between intersection and union of predicted and reference pixels per class; and (6) mean IoU, i.e., the mean value of IoU across all classes (Maxwell et al. 2021). For each dataset, metrics were computed over all classes present in its reference ground truth dataset (Section 2.2).

To assess whether a post-processing step could improve output maps, we applied a sieve filter, which reduces the salt-and-pepper effect. We tested different sieve values on UAV-derived maps: 25 pixels (i.e., removing patches $< 0.01\,m^2$ and assigning those pixels to the neighboring class), 100 pixels (i.e., removing patches $< 0.04\,m^2$), and 250 pixels (i.e., removing patches $< 0.10\,m^2$), and compared the resulting map accuracy metrics.

Finally, to distinguish temporal and dataset-specific effects on performance, we performed a cross-temporal test using remote sensing imagery (Appendix S14).

3 | Results and Discussion

Habitat maps produced through segmentation of RGB imagery are shown in Figure 3, whereas those derived from multispectral

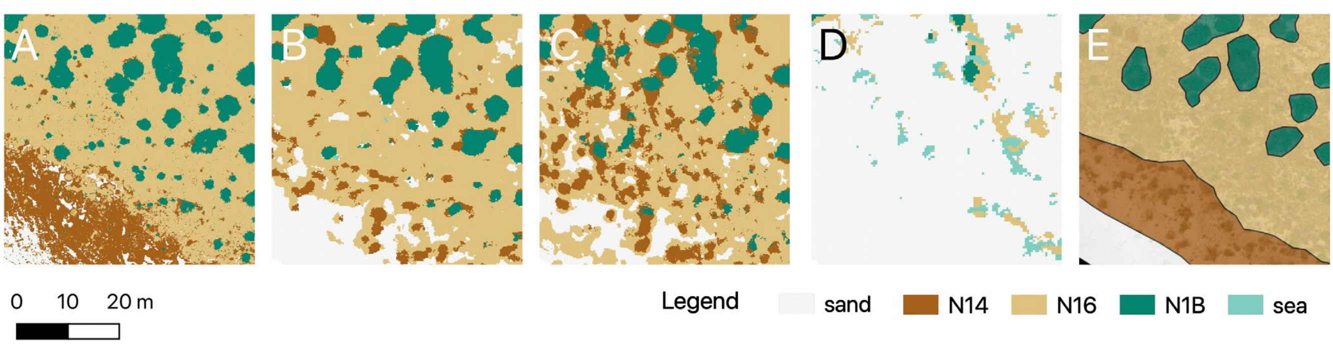

FIGURE 3 | Close-up views of the habitat maps produced through CNN segmentation of RGB imagery from four datasets: UAV (A), airborne (B), Google Earth (C), and WorldView-3 (D), and of the visually delineated ground truth map (E).

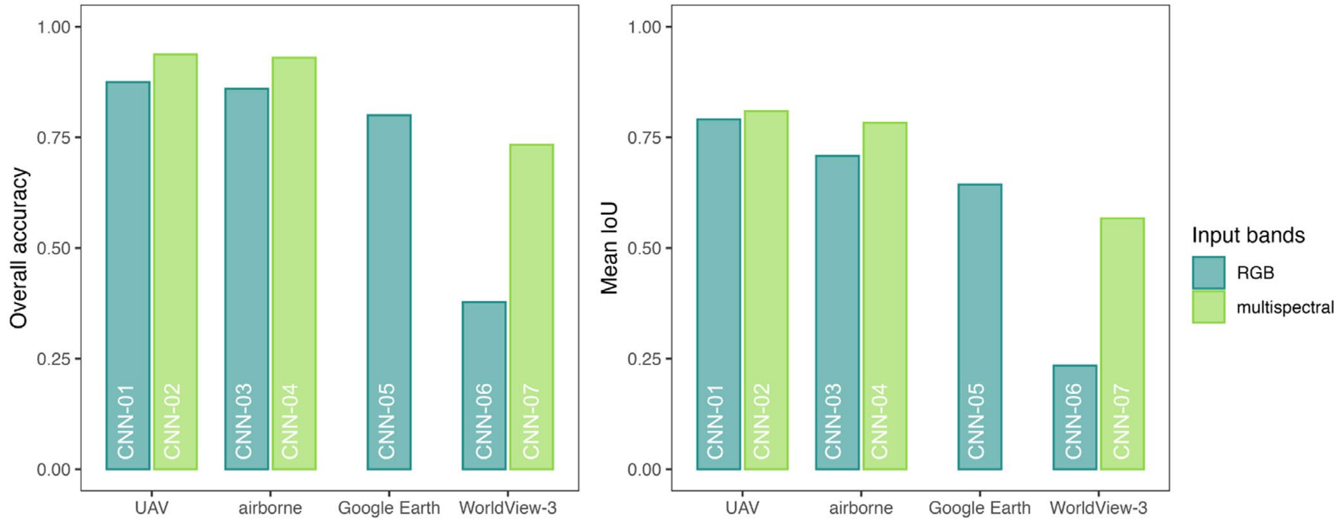

FIGURE 4 | Overall accuracy and mean intersection over union (IoU) of the CNN-classified maps.

imagery are shown in Appendix S3. Despite visible differences in terms of resolution and noise, in most cases the typical sea-inland succession can be recognized (Appendix S4), with bare sand and shifting dunes closer to the sea, followed by stable dune grasslands intermixed with dune scrubs (Acosta et al. 2007), reflecting the typical changes in environmental conditions and plant diversity along the sea-inland gradient (Torca et al. 2019; Tordoni et al. 2021).

Overall, four out of seven maps had high accuracy (overall accuracy > 85% and mean IoU > 70%; Figure 4), confirming the potential of CNNs for habitat mapping, specifically for their ability to implicitly learn spatial patterns and textures, which are known to enhance vegetation classification (e.g., Bhatt et al. 2022). To our knowledge, this is one of the first studies to assess the use of CNNs for mapping habitats on coastal dunes. For comparison, Suo et al. (2019) mapped land cover with a maximum likelihood classifier achieving 69% accuracy with RGB and 78% with multispectral UAV imagery. Agrillo et al. (2023) reached 78% accuracy combining UAV data with environmental predictors in a Random Forest model. Similarly, Laporte-Fauret et al. (2020) applied Random Forest to hyperspectral data, producing vegetation maps with 83% accuracy.

A key finding of this study is the consistent decline in CNN performance with decreasing spatial resolution: overall accuracy of RGB-based maps dropped from 88% (UAV) to 86% (airborne), 80% (Google Earth), and 38% (WorldView-3). Similarly, mean IoU dropped from 79% (UAV) to 71% (airborne), 64% (Google Earth), and 23% (WorldView-3). This trend is in line with previous research on CNNs. For example, tree mapping accuracy in a temperate forest decreased from 89% at 0.02 m to 62% at 0.32 m (Schiefer et al. 2020), whereas accuracy in a bamboo forest decreased from 93% at 0.13 m to 74% at 0.65 m (Watanabe et al. 2020).

This resolution effect suggests that only hyperspatial imagery, i.e., imagery with pixels much smaller than target objects, can reveal the fine-scale patterns that CNNs exploit to identify objects, such as branching structures for trees (Schiefer et al. 2020). Notably, the benefits of hyperspatial data do not apply to all methods. For example, conventional spectral-based classifiers may perform worse with higher resolution data due to high intra-class spectral variability (e.g., sunlit and shaded leaves of the same tree having different reflectance), which reduces spectral separability (Nagendra and Rocchini 2008). Conversely, their performance can improve as resolution decreases and spectral separability increases (De Giglio et al. 2017), until mixed pixels become prevalent, at which point pixel-based fuzzy classifications may be preferable (Pafumi et al. 2025).

Additionally, the negative impact of low spatial resolution on CNN performance may be amplified by an indirect effect: to match field plot sizes, patches extracted from lower resolution imagery had a smaller number of pixels. Smaller tile sizes can increase the edge effect caused by the moving window approach of CNNs, as noted by Schiefer et al. (2020), although they reported only minor performance differences across tile sizes (128, 256, 512 pixels).

Interestingly, including additional spectral bands had only a minor positive effect on mapping accuracy at very high resolutions (+6 percentage points for UAV, +7 for airborne), whereas the effect was greater at coarser resolutions (+35 percentage points for WorldView-3). This suggests that spatial patterns may be more informative than spectral reflectance for mapping at very high resolutions, as previous research has found (e.g., Carbonneau et al. 2020), highlighting the value of relatively inexpensive RGB sensors on UAVs.

It is important to note that the remote sensing datasets considered in this study differed not only in spatial and spectral resolution but also in the time gap separating their acquisition from ground truth data collection. Despite the general ecological and morphological stability of the study area, lower performance was observed for the dataset with the largest time gap (5 years), suggesting a potential limit to the temporal resilience of the habitat mapping models, possibly more evident for the more dynamic habitats. Future studies specifically addressing the temporal decay of model performance in coastal dune environments will be essential to derive practical guidance, as has been done, for example, for forest areas (McRoberts et al. 2016).

We observed a marked difference in classification performance among habitats, especially at coarser resolutions (Appendix S5). Dune scrubs (habitat N1B) were mapped with the highest precision and recall, as in other studies (Marzialetti et al. 2019; Pafumi et al. 2025). Stable dune grasslands (N16) also reached relatively high values, whereas shifting dunes (N14) often achieved a precision similar to N16 but a low recall, mostly due to confusion with bare sand (Appendices S6, S7). These two habitats showed the greatest decline in accuracy with decreasing resolution, probably because the fine-scale patterns exploited by CNNs were no longer discernible, also due to their lower vegetation cover (Appendix S8).

Furthermore, we found that a simple post-processing step reduced the salt-and-pepper effect in the highest resolution maps, slightly improving accuracy (Appendices S9, S10). However, the advisability of applying this step, including the choice of optimal filter size, depends on the application, and more sophisticated methods could be explored (Chen et al. 2018).

Although this study focused on a single site, the findings have broader implications for large-scale applications. Ideally, extensive UAV surveys would provide the most accurate habitat maps for coastal dunes. Thanks to the high spatial detail of these images, field sampling efforts can also be reduced. We surveyed a relatively small number of plots (65 plots over 4 ha) and then expanded the ground truth dataset through photo interpretation. Notably, several studies have reported higher accuracy using visually delineated ground truth from imagery compared to field-based data, due to reduced spatial inaccuracy and sampling bias (Kattenborn et al. 2019; Marzialetti et al. 2019). However, field surveys remain necessary to relate vegetation features to their appearance in imagery, especially if plot locations are recorded with high precision simultaneously with UAV acquisition, as in this work, thus minimizing spatial misalignment.

Despite these advantages, UAVs are currently not appropriate for covering broad spatial extents, such as the whole Italian coastline, due to the required costs and expertise. Nonetheless, UAV-based research has been increasing in recent years (e.g., Agrillo et al. 2023; Belcore et al. 2024; De Giglio et al. 2019; Innangi et al. 2025; Malavasi et al. 2021; Marzialetti et al. 2021), and new opportunities may emerge in the future.

As an alternative, our study showed that airborne and Google Earth imagery can still offer reliable maps, though only the latter is currently available at the national level. Based on these results, a national-scale test of CNNs using these data will be the next step in research. It is important to note, however, that the transferability of CNNs across sites can vary, from low (Watanabe et al. 2020) to high (Carbonneau et al. 2020; Schiefer et al. 2020), indicating the need for future studies to specifically assess CNN transferability in coastal dunes. In particular, the requirement for site-specific calibration, which could constrain broad-scale applications, could be addressed by first training a model on a large and diverse ground truth dataset representing a variety of ecological conditions, and then adapting the model to specific local conditions through transfer learning, thus requiring a minimal amount of additional data, as has been done, for example, for rivers worldwide (Carbonneau et al. 2020).

In the application of this methodology to different sites, the temporal aspect should also be considered. Here, we used one image for each remote sensing data source, selecting the vegetation growing season as the optimal period for image acquisition, as spectral differences between dune vegetation types are enhanced (Cruz et al. 2023). In other seasons, confusion between vegetation and substrate may increase due to senescence or dormancy, and habitat discrimination can be affected. However, multi-temporal models could also be developed in the future, building on evidence from other studies suggesting that coastal dune vegetation classes show different seasonal patterns of spectral vegetation indices (Marzialetti et al. 2019) and temporal heterogeneity indices (Marzialetti et al. 2020), and thus that multi-temporal information could further improve habitat discrimination.

Moreover, some coastal dune systems have large amounts of woody debris and marine litter (Andriolo et al. 2020). Here, their presence was limited and, when present, thanks to their white color and high reflectance, these objects were generally assigned to the bare sand class, thus minimizing classification noise. However, these elements should be considered when applying the methodology to other sites.

By providing methodological indications on habitat mapping on coastal dunes, this work can support a wide range of practical applications, including monitoring of restoration actions (e.g., Fabbri et al. 2021; Gracia et al. 2025; Haskins et al. 2021), informing ecomorphodynamic studies (Yousefi Lalimi et al. 2017), and contributing to model calibration (e.g., Camporeale and Latella 2025). Moreover, high-resolution habitat maps are essential in the context of European policies, for example, to support mandatory reporting under the Habitats Directive and to provide quantitative data required by the Nature Restoration Regulation (European Parliament and Council 2024).

4 | Conclusion

This study emphasizes the efficacy of CNNs for mapping coastal dune habitats and offers a pioneering analysis of the influence of the spatial resolution of remote sensing data on CNN performance. Very high-resolution UAV imagery was confirmed as the most valuable data source for producing accurate habitat maps, revealing fine-scale spatial patterns that are essential for CNNs. With coarser-resolution datasets, mapping accuracy clearly declined, whereas the inclusion of additional spectral bands became more beneficial. Despite not being the ideal solution, airborne and Google Earth data still supported high-accuracy maps ($\geq$80%), suggesting potential for cost-effective, broader-scale applications, once CNN transferability across dune systems has been further explored. By assessing CNN applicability across multiple remote sensing datasets, this study offers novel and practical insights that can support monitoring and conservation of the highly vulnerable coastal dune ecosystems.

Author Contributions

G.B., S.M., E.P., and D.R. conceived the research idea. L.S., S.M., and E.P. collected field data. L.S. collected and processed UAV data. E.P. and

E.T. carried out the analyses, with support from G.B. and D.R. for the methodology and from C.A., G.B., L.S., E.F., T.F., D.R., and S.M. for the interpretation of the results. E.P. wrote the first draft. C.A., G.B., L.S., E.F., T.F., D.R., and S.M. contributed to the writing. All authors critically revised the manuscript and gave final approval for publication.

Acknowledgments

We thank the Maremma Regional Park for granting research permits and supporting fieldwork activities. We are grateful to Paul Toffoloni for his assistance with the code. WorldView-3 data were provided by the European Space Agency (ESA) within its Third Party Missions programme. Open access publishing facilitated by Universita degli Studi di Trieste, as part of the Wiley - CRUI-CARE agreement.

Funding

E.P., C.A., E.F., and S.M. were funded under the National Recovery and Resilience Plan (NRRP), Mission 4 Component 2 Investment 1.4—Call for tender No. 3138 of December 16, 2021, rectified by Decree n.3175 of December 18, 2021, of the Italian Ministry of University and Research funded by the European Union—NextGenerationEU; Award Number: Project code CN_00000033, Concession Decree No. 1034 of June 17, 2022, adopted by the Italian Ministry of University and Research, CUP B63C22000650007, Project title "National Biodiversity Future Center—NBFC."D.R. acknowledges funding from the B3 project (Biodiversity Building Blocks for policy), funded by the European Union's Horizon Europe Research and Innovation Programme (Grant Agreement No. 101059592). The views and opinions expressed are those of the author only and do not necessarily reflect those of the European Union or the European Commission. Neither the European Union nor the European Commission can be held responsible for them.

Conflicts of Interest

The authors declare no conflicts of interest.

Data Availability Statement

The code and ground truth data used for the analyses are available at https://github.com/emiliapafumi/deep-dunes. Remote sensing data can be accessed as described in the text: the airborne orthophoto is available from https://www.regione.toscana.it/geoscopio; Google Earth imagery can be downloaded from Google Earth Pro; WorldView-3 data can be requested from https://earth.esa.int/eogateway/missions/worldview-3 after approval of a data request to the European Space Agency.

References

EEC. 1992. "Council Directive 92/43/EEC of 21 May 1992 on the Conservation of Natural Habitats and of Wild Fauna and Flora." *Official Journal of the European Communities* L 206: 7–50.

Abadi, M., A. Agarwal, P. Barham, et al. 2015. "TensorFlow: Large-Scale Machine Learning on Heterogeneous Systems." tensorflow.org.

Acosta, A., S. Ercole, A. Stanisci, V. D. P. Pillar, and C. Blasi. 2007. "Coastal Vegetation Zonation and Dune Morphology in Some Mediterranean Ecosystems." *Journal of Coastal Research* 23: 1518–1524. https://doi.org/10.2112/05-0589.1.

Agrillo, E., F. Filipponi, R. Salvati, A. Pezzarossa, and L. Casella. 2023. "Modeling Approach for Coastal Dune Habitat Detection on Coastal Ecosystems Combining Very High-Resolution UAV Imagery and Field Survey." *Remote Sensing in Ecology and Conservation* 9: 251–267. https://doi.org/10.1002/rse2.308.

Airbus. 2023. "Pléiades Neo Satellite Imagery of 26 April 2023." Google Earth Pro 2025.

Andriolo, U., G. Gonçalves, F. Bessa, and P. Sobral. 2020. "Mapping Marine Litter on Coastal Dunes With Unmanned Aerial Systems: A Showcase on the Atlantic Coast." *Science of the Total Environment* 736: 139632. https://doi.org/10.1016/j.scitotenv.2020.139632.

Beccari, E., C. Pérez Carmona, E. Tordoni, et al. 2024. "Plant Spectral Diversity From High-Resolution Multispectral Imagery Detects Functional Diversity Patterns in Coastal Dune Communities." *Journal of Vegetation Science* 35: e13239. https://doi.org/10.1111/jvs.13239.

Belcore, E., M. Latella, M. Piras, and C. Camporeale. 2024. "Enhancing Precision in Coastal Dunes Vegetation Mapping: Ultra-High Resolution Hierarchical Classification at the Individual Plant Level." *International Journal of Remote Sensing* 45: 4527–4552. https://doi.org/10.1080/01431161.2024.2354135.

Bhatt, P., A. Maclean, Y. Dickinson, and C. Kumar. 2022. "Fine-Scale Mapping of Natural Ecological Communities Using Machine Learning Approaches." *Remote Sensing* 14, no. 3: 563. https://doi.org/10.3390/rs14030563.

Bruelheide, H., L. Tichý, M. Chytrý, and F. Jansen. 2021. "Implementing the Formal Language of the Vegetation Classification Expert Systems (ESy) in the Statistical Computing Environment R." *Applied Vegetation Science* 24: e12562. https://doi.org/10.1111/avsc.12562.

Camporeale, C., and M. Latella. 2025. "Stochastic Dynamics of Coastal Dune Vegetation." *JGR Earth Surface* 130: e2025JF008610. https://doi.org/10.1029/2025JF008610.

Carbonneau, P. E., S. J. Dugdale, T. P. Breckon, et al. 2020. "Adopting Deep Learning Methods for Airborne RGB Fluvial Scene Classification." *Remote Sensing of Environment* 251: 112107. https://doi.org/10.1016/j.rse.2020.112107.

Chen, L.-C., G. Papandreou, I. Kokkinos, K. Murphy, and A. L. Yuille. 2018. "DeepLab: Semantic Image Segmentation With Deep Convolutional Nets, Atrous Convolution, and Fully Connected CRFs." *IEEE Transactions on Pattern Analysis and Machine Intelligence* 40: 834–848. https://doi.org/10.1109/TPAMI.2017.2699184.

Chollet, F. 2015. "Keras." https://keras.io.

Chytrý, M., L. Tichý, S. M. Hennekens, et al. 2020. "EUNIS Habitat Classification: Expert System, Characteristic Species Combinations and Distribution Maps of European Habitats." *Applied Vegetation Science* 23: 648–675. https://doi.org/10.1111/avsc.12519.

Cipriano, C., S. Noce, S. Mereu, and M. Santini. 2025. "Algorithms Going Wild—A Review of Machine Learning Techniques for Terrestrial Ecology." *Ecological Modelling* 506: 111164. https://doi.org/10.1016/j.ecolmodel.2025.111164.

Corbane, C., S. Lang, K. Pipkins, et al. 2015. "Remote Sensing for Mapping Natural Habitats and Their Conservation Status—New Opportunities and Challenges." *International Journal of Applied Earth Observation and Geoinformation* 37: 7–16. https://doi.org/10.1016/j.jag.2014.11.005.

Cresson, R. 2019. "A Framework for Remote Sensing Images Processing Using Deep Learning Techniques." *IEEE Geoscience and Remote Sensing Letters* 16: 25–29. https://doi.org/10.1109/LGRS.2018.2867949.

Cresson, R. 2020. *Deep Learning for Remote Sensing Images With Open Source Software*. 1st ed. CRC Press. https://doi.org/10.1201/9781003020851.

Cruz, C., J. O'Connell, K. McGuinness, J. R. Martin, P. M. Perrin, and J. Connolly. 2023. "Assessing the Effectiveness of UAV Data for Accurate Coastal Dune Habitat Mapping." *European Journal of Remote Sensing* 56: 2191870. https://doi.org/10.1080/22797254.2023.2191870.

De Giglio, M., F. Goffo, N. Greggio, N. Merloni, M. Dubbini, and M. Barbarella. 2017. "Satellite and Unmanned Aerial Vehicle Data for the Classification of Sand Dune Vegetation." *International Archives of the Photogrammetry, Remote Sensing and Spatial Information*

Sciences XLII-3/W2: 43–50. https://doi.org/10.5194/isprs-archives-XLII-3-W2-43-2017.

De Giglio, M., N. Greggio, F. Goffo, N. Merloni, M. Dubbini, and M. Barbarella. 2019. "Comparison of Pixel- and Object-Based Classification Methods of Unmanned Aerial Vehicle Data Applied to Coastal Dune Vegetation Communities: Casal Borsetti Case Study." *Remote Sensing* 11: 1416. https://doi.org/10.3390/rs11121416.

Delbosc, P., I. Lagrange, C. Rozo, et al. 2021. "Assessing the Conservation Status of Coastal Habitats Under Article 17 of the EU Habitats Directive." *Biological Conservation* 254: 108935. https://doi.org/10.1016/j.biocon.2020.108935.

Eltner, A., A. Kaiser, C. Castillo, G. Rock, F. Neugirg, and A. Abellán. 2016. "Image-Based Surface Reconstruction in Geomorphometry—Merits, Limits and Developments." *Earth Surface Dynamics* 4: 359–389. https://doi.org/10.5194/esurf-4-359-2016.

European Parliament and Council. 2024. "Regulation (EU) 2024/1991 of the European Parliament and of the Council of 24 June 2024 on Nature Restoration and Amending Regulation (EU) 2022/869." *Official Journal of the European Union* L 2024/1991.

Fabbri, S., E. Grottoli, C. Armaroli, and P. Ciavola. 2021. "Using High-Spatial Resolution UAV-Derived Data to Evaluate Vegetation and Geomorphological Changes on a Dune Field Involved in a Restoration Endeavour." *Remote Sensing* 13: 1987. https://doi.org/10.3390/rs13101987.

Fromm, M., M. Schubert, G. Castilla, J. Linke, and G. McDermid. 2019. "Automated Detection of Conifer Seedlings in Drone Imagery Using Convolutional Neural Networks." *Remote Sensing* 11: 2585. https://doi.org/10.3390/rs11212585.

GDAL/OGR contributors. 2026. "GDAL/OGR Geospatial Data Abstraction software Library". Open Source Geospatial Foundation. https://doi.org/10.5281/zenodo.5884351.

Google. 2025. "Google Earth Pro (Version 7.3.6)." https://www.google.com/earth/versions/.

Gracia, V., M. M. Dietrich, J. P. Sierra, et al. 2025. "Using UAVs to Monitor the Evolution of Restored Coastal Dunes." *Remote Sensing* 17: 3263. https://doi.org/10.3390/rs17193263.

Grizonnet, M., J. Michel, V. Poughon, J. Inglada, M. Savinaud, and R. Cresson. 2017. "Orfeo ToolBox: Open Source Processing of Remote Sensing Images." *Open Geospatial Data, Software and Standards* 2: 15. https://doi.org/10.1186/s40965-017-0031-6.

Guirado, E., S. Tabik, D. Alcaraz-Segura, J. Cabello, and F. Herrera. 2017. "Deep-Learning Versus OBIA for Scattered Shrub Detection With Google Earth Imagery: *Ziziphus lotus* as Case Study." *Remote Sensing* 9: 1220. https://doi.org/10.3390/rs9121220.

Haskins, J., C. Endris, A. S. Thomsen, F. Gerbl, M. C. Fountain, and K. Wasson. 2021. "UAV to Inform Restoration: A Case Study From a California Tidal Marsh." *Frontiers in Environmental Science* 9: 642906. https://doi.org/10.3389/fenvs.2021.642906.

Innangi, M., M. Di Febbraro, M. Balsi, et al. 2025. "A Novel High-Resolution Eco-Functional Vegetation Mapping of Coastal Dunes." *Ecological Indicators* 171: 113157. https://doi.org/10.1016/j.ecolind.2025.113157.

Innangi, M., F. Marzialetti, M. Di Febbraro, et al. 2023. "Coastal Dune Invaders: Integrative Mapping of *Carpobrotus* sp. Pl. (Aizoaceae) Using UAVs." *Remote Sensing* 15: 503. https://doi.org/10.3390/rs15020503.

Kattenborn, T., J. Eichel, and F. E. Fassnacht. 2019. "Convolutional Neural Networks Enable Efficient, Accurate and Fine-Grained Segmentation of Plant Species and Communities From High-Resolution UAV Imagery." *Scientific Reports* 9: 17656. https://doi.org/10.1038/s41598-019-53797-9.

Kattenborn, T., J. Leitloff, F. Schiefer, and S. Hinz. 2021. "Review on Convolutional Neural Networks (CNN) in Vegetation Remote Sensing." *ISPRS Journal of Photogrammetry and Remote Sensing* 173: 24–49. https://doi.org/10.1016/j.isprsjprs.2020.12.010.

Kerry, R. G., F. J. P. Montalbo, R. Das, et al. 2022. "An Overview of Remote Monitoring Methods in Biodiversity Conservation." *Environmental Science and Pollution Research* 29: 80179–80221. https://doi.org/10.1007/s11356-022-23242-y.

Kuester, M. 2016. *Radiometric Use of WorldView-3 Imagery*. DigitalGlobe.

Lansu, E. M., V. C. Reijers, F. Daniëls, R. James, M. J. A. Christianen, and T. Van Der Heide. 2025. "Habitat Mapping of Coastal Dunes With Deep Learning." *Ecological Informatics* 92: 103444. https://doi.org/10.1016/j.ecoinf.2025.103444.

Laporte-Fauret, Q., B. Lubac, B. Castelle, et al. 2020. "Classification of Atlantic Coastal Sand Dune Vegetation Using In Situ, UAV, and Airborne Hyperspectral Data." *Remote Sensing* 12: 2222. https://doi.org/10.3390/rs12142222.

Latella, M., A. Luijendijk, A. M. Moreno-Rodenas, and C. Camporeale. 2021. "Satellite Image Processing for the Coarse-Scale Investigation of Sandy Coastal Areas." *Remote Sensing* 13: 4613. https://doi.org/10.3390/rs13224613.

LeCun, Y., Y. Bengio, and G. Hinton. 2015. "Deep Learning." *Nature* 521: 436–444. https://doi.org/10.1038/nature14539.

Malavasi, M. 2020. "The Map of Biodiversity Mapping." *Biological Conservation* 252: 108843. https://doi.org/10.1016/j.biocon.2020.108843.

Malavasi, M., M. Bazzichetto, J. Komárek, et al. 2021. "Unmanned Aerial Systems-Based Monitoring of the Eco-Geomorphology of Coastal Dunes Through Spectral Rao's Q." *Applied Vegetation Science* 24: e12567. https://doi.org/10.1111/avsc.12567.

Marzialetti, F., M. Di Febbraro, M. Malavasi, S. Giulio, A. T. R. Acosta, and M. L. Carranza. 2020. "Mapping Coastal Dune Landscape Through Spectral Rao's Q Temporal Diversity." *Remote Sensing* 12: 2315. https://doi.org/10.3390/rs12142315.

Marzialetti, F., L. Frate, W. De Simone, A. R. Frattaroli, A. T. R. Acosta, and M. L. Carranza. 2021. "Unmanned Aerial Vehicle (UAV)-Based Mapping of *Acacia saligna* Invasion in the Mediterranean Coast." *Remote Sensing* 13: 3361. https://doi.org/10.3390/rs13173361.

Marzialetti, F., S. Giulio, M. Malavasi, M. G. Sperandii, A. T. R. Acosta, and M. L. Carranza. 2019. "Capturing Coastal Dune Natural Vegetation Types Using a Phenology-Based Mapping Approach: The Potential of Sentinel-2." *Remote Sensing* 11: 1506. https://doi.org/10.3390/rs11121506.

Maxwell, A. E., T. A. Warner, and L. A. Guillén. 2021. "Accuracy Assessment in Convolutional Neural Network-Based Deep Learning Remote Sensing Studies—Part 1: Literature Review." *Remote Sensing* 13: 2450. https://doi.org/10.3390/rs13132450.

McRoberts, R. E., E. Næsset, and T. Gobakken. 2016. "The Effects of Temporal Differences Between Map and Ground Data on Map-Assisted Estimates of Forest Area and Biomass." *Annals of Forest Science* 73: 839–847. https://doi.org/10.1007/s13595-015-0485-6.

Nagendra, H., and D. Rocchini. 2008. "High Resolution Satellite Imagery for Tropical Biodiversity Studies: The Devil Is in the Detail." *Biodiversity and Conservation* 17: 3431–3442. https://doi.org/10.1007/s10531-008-9479-0.

Nezami, S., E. Khoramshahi, O. Nevalainen, I. Pölönen, and E. Honkavaara. 2020. "Tree Species Classification of Drone Hyperspectral and RGB Imagery With Deep Learning Convolutional Neural Networks." *Remote Sensing* 12: 1070. https://doi.org/10.3390/rs12071070.

Nourisson, D. H., and F. Scapini. 2015. "Seasonal Variation in the Orientation of *Talitrus saltator* on a Mediterranean Sandy Beach: An

Ecological Interpretation." *Ethology Ecology & Evolution* 27: 277–293. https://doi.org/10.1080/03949370.2014.946538.

Pafumi, E., C. Angiolini, G. Bacaro, et al. 2025. "Fuzzy Approaches Provide Improved Spatial Detection of Coastal Dune EU Habitats." *Ecological Informatics* 86: 103059. https://doi.org/10.1016/j.ecoinf.2025.103059.

Pérez-Carabaza, S., O. Boydell, and J. O'Connell. 2021. "Habitat Classification Using Convolutional Neural Networks and Multitemporal Multispectral Aerial Imagery." *Journal of Applied Remote Sensing* 15: 42406. https://doi.org/10.1117/1.JRS.15.042406.

Pesaresi, S., E. Biondi, and S. Casavecchia. 2017. "Bioclimates of Italy." *Journal of Maps* 13: 955–960. https://doi.org/10.1080/17445647.2017.1413017.

Pranzini, E., I. Cinelli, and G. Anfuso. 2024. "Beaches' Expulsion From Paradise: From a Natural to an Artificial Littoral in Tuscany (Italy)." *Coasts* 4: 697–725. https://doi.org/10.3390/coasts4040037.

QGIS Development Team. 2024. "QGIS Geographic Information System." https://qgis.org.

Regione Toscana. 2023. "Ortofoto 2023 - Base Informativa Territoriale Regionale, Art. 55 L.R. 65/2014." https://www502.regione.toscana.it/geoscopio/ortofoto.html.

Ronneberger, O., P. Fischer, and T. Brox. 2015. "U-Net: Convolutional Networks for Biomedical Image Segmentation." In *Medical Image Computing and Computer-Assisted Intervention—MICCAI 2015*, edited by N. Navab, J. Hornegger, W. M. Wells, and A. F. Frangi, 234–241. Lecture Notes in Computer Science. Springer International Publishing. https://doi.org/10.1007/978-3-319-24574-4_28.

Saltiel, T. M., P. E. Dennison, M. J. Campbell, T. R. Thompson, and K. R. Hambrecht. 2022. "Tradeoffs Between UAS Spatial Resolution and Accuracy for Deep Learning Semantic Segmentation Applied to Wetland Vegetation Species Mapping." *Remote Sensing* 14: 2703. https://doi.org/10.3390/rs14112703.

Sarmati, S., C. Angiolini, M. G. Sperandii, et al. 2025. "A Complex Interplay Between Natural and Anthropogenic Factors Shapes Plant Diversity Patterns in Mediterranean Coastal Dunes." *Landscape Ecology* 40: 20. https://doi.org/10.1007/s10980-024-02025-5.

Schiefer, F., T. Kattenborn, A. Frick, et al. 2020. "Mapping Forest Tree Species in High Resolution UAV-Based RGB-Imagery by Means of Convolutional Neural Networks." *ISPRS Journal of Photogrammetry and Remote Sensing* 170: 205–215. https://doi.org/10.1016/j.isprsjprs.2020.10.015.

Suo, C., E. McGovern, and A. Gilmer. 2019. "Coastal Dune Vegetation Mapping Using a Multispectral Sensor Mounted on an UAS." *Remote Sensing* 11: 1814. https://doi.org/10.3390/rs11151814.

Torca, M., J. A. Campos, and M. Herrera. 2019. "Changes in Plant Diversity Patterns Along Dune Zonation in South Atlantic European Coasts." *Estuarine, Coastal and Shelf Science* 218: 39–47. https://doi.org/10.1016/j.ecss.2018.11.016.

Tordoni, E., G. Bacaro, P. Weigelt, et al. 2021. "Disentangling Native and Alien Plant Diversity in Coastal Sand Dune Ecosystems Worldwide." *Journal of Vegetation Science* 32: e12861. https://doi.org/10.1111/jvs.12961.

Tordoni, E., F. Petruzzellis, A. Nardini, T. Savi, and G. Bacaro. 2019. "Make It Simpler: Alien Species Decrease Functional Diversity of Coastal Plant Communities." *Journal of Vegetation Science* 30: 498–509. https://doi.org/10.1111/jvs.12734.

Watanabe, S., K. Sumi, and T. Ise. 2020. "Identifying the Vegetation Type in Google Earth Images Using a Convolutional Neural Network: A Case Study for Japanese Bamboo Forests." *BMC Ecology* 20: 65. https://doi.org/10.1186/s12898-020-00331-5.

Yousefi Lalimi, F., S. Silvestri, L. J. Moore, and M. Marani. 2017. "Coupled Topographic and Vegetation Patterns in Coastal Dunes: Remote Sensing Observations and Ecomorphodynamic Implications." *JGR Biogeosciences* 122: 119–130. https://doi.org/10.1002/2016JG003540.

Zhao, X., Y. Yuan, M. Song, et al. 2019. "Use of Unmanned Aerial Vehicle Imagery and Deep Learning UNet to Extract Rice Lodging." *Sensors* 19: 3859. https://doi.org/10.3390/s19183859.

Supporting Information

Additional supporting information can be found online in the Supporting Information section. **Appendix S1:** Scheme of the CNN architecture used in this study for the UAV dataset and for the other datasets. **Appendix S2:** Validation loss of CNN models trained on different datasets across learning epochs. **Appendix S3:** Close-up views of the habitat maps produced through CNN segmentation of multispectral imagery from three datasets: UAV, airborne, and WorldView-3. **Appendix S4:** Habitat maps of the whole study area produced from CNN models trained on different datasets, and a ground truth map produced by visual interpretation of the highest-resolution imagery. **Appendix S5:** Class-specific accuracy metrics for each CNN model: precision (i.e., proportion of true positives over all classified positives), recall (i.e., proportion of true positives over all actual positives), F1-score (i.e., harmonic mean of precision and recall), and IoU (intersection over union). **Appendix S6:** Confusion matrices for CNN models. **Appendix S7:** Percentage cover of each class in the habitat maps of the study area produced by the CNN models trained on different datasets, and in the ground truth map produced by visual interpretation. **Appendix S8:** Boxplot of the total vegetation cover recorded in the field-surveyed plots, assigned to three EUNIS habitats: shifting dunes (N14), dune grasslands (N16), and dune scrub (N1B). **Appendix S9:** Close-up views of the habitat maps produced from CNN-01 and CNN-02. The panels represent the output map before and after a post-processing step, consisting in the application of a sieve filter removing patches with <25 pixels, <100 pixels, and <250 pixels. **Appendix S10:** Accuracy metrics for habitat maps derived from UAV imagery, before and after applying post-processing sieve filters (25, 100, 250 pixels). **Appendix S11:** Description of the habitat classes considered in this study. Diagnostic species are derived from EUNIS habitat description (Chytrý et al. 2020), with species names updated according to the Portal to the Flora of Italy (2026). **Appendix S12:** Number of pixels for each class in the reference ground truth dataset derived from each remote sensing data source. **Appendix S13:** Location of the field-surveyed transects (coordinates are reported for the first and the last plot of each transect). **Appendix S14:** Comparison of remote sensing images and CNN-classified maps across different years and datasets to assess temporal versus dataset-driven differences.